Power consumption and circulation flow rate of polymer solutions in a stirred vessel powered by an hyperboloid impeller

A. S. Cavadas(1) and F. T. Pinho(2)

Centro de Estudos de Fenómenos de Transporte, DEMEGI

Faculdade de Engenharia, Universidade do Porto

Rua Dr. Roberto Frias, 4200-465 Porto, Portugal

(1)E-mail:adelioc@fe.up.pt, (2)E-mail: fpinho@fe.up.pt

ABSTRACT

An investigation was carried out to determine the power consumption, the circulating flow rate and the circulating efficiency in stirred vessel flows powered by an hyperboloid impeller. The fluids tested were dilute and semi-dilute aqueous solutions of tylose, CMC and xanthan gum (XG) at weight concentrations ranging from 0.1% to 0.6% and the solutions had varying degrees of shear-thinning and elasticity. At Reynolds numbers in the range 10^3 to 10^4 the power number has the lowest values, of the order of 0.7 and less, whereas for Newtonian fluids it is higher than the asymptotic high Reynolds number value of 0.81, so the power reduction never exceeded 13% in comparison to the Newtonian behaviour.

The measurements of the axial velocity across radial planes located above the impeller base, at around z/R=1, were carried out at Reynolds numbers of 5,400 and 8,200 for solutions of 0.2% CMC and 0.2% XG, respectively. For comparison purposes measurements with water were also carried out, but here the Reynolds numbers were of 56,200 and 93,600. Whereas for the water flow the circulating flow number Fl_c varied from 0.51 to 0.54, there was a decrease of about 20% for both the 0.2% CMC and 0.2% XG polymer solutions which showed values of Fl_c = 0.42 and 0.45, respectively. Thus, the reduction is the circulating flow number was twice that found in the power number and consequently there was a decrease in the efficiency number.

The velocity measurements also showed a severe reduction in turbulence intensity at the wall jet for the 0.2% xanthan gum solution whereas for the 0.2% CMC the decrease in turbulence was mild (~10% relative to the Newtonian turbulence values). This different turbulent flow behaviour of the xanthan gum was attributed to its intense shear-thinning, especially at low shear rates.

1. INTRODUCTION

Stirred vessels are common in the process industry where they fulfil a large variety of tasks from the mixing of liquids and suspensions to blending, with and without aeration, and often including heat and mass transfer. The various objectives entail different vessel shapes and types of agitator from the bulky low rotational speed impellers, required for very viscous fluids, to small high speed rotating devices for low viscosity fluids. The use of hyperboloid impellers is advantageous in processes involving low viscosity fluids and microorganisms, one such case being waste water treatment plants. This advantage stems from the capacity of the hyperboloid to sustain an overall gentle flow that avoids destruction of useful microorganisms (Höfken et al, 1991, 1994) at the same time that it provides a reasonable degree of mixing with a fairly low level of power consumption. Given its application in waste water treatment plants, which deal with non-Newtonian fluids (Monteiro and Valente, 1996) it is necessary to extend previous investigations with Newtonian fluids by Höfken et al (1991, 1994), Pinho et al (1997, 2000), Nouri and Whitelaw (1994) and Ismailov et al (1997) to low viscosity non-Newtonian fluids, and later to solid-liquid and solid-liquid-gas flows.

In this work we report results of a preliminary investigation on the behaviour of dilute and semi-dilute polymer solutions in stirred vessel flows powered by hyperboloid impellers. The investigation concentrates on measurements of the power consumption for the various polymer solutions and radial profiles of axial velocity for some selected cases aimed at calculating the circulation flow rate and in order to determine hydrodynamic efficiency parameters.

The theory underlying the various measurements is presented in the next section and is followed by a description of the experimental facility and instrumentation in Section 3. Prior to the discussion of the results, the rheological characteristics of the fluids are presented. A summary of the main conclusions closes the paper.

2. THEORY

The power consumption in a stirred vessel depends on fluid properties, geometrical parameters and flow quantities and the functional relationship amongst these quantities can be normalised for single-phase fluids as,

$$Ne \equiv \frac{P}{\rho N^3 D^5} = f\left(\frac{\rho N D^2}{\eta_c}, \frac{N^2 D}{g}, \frac{D}{T}, \frac{C}{T}, \frac{H}{T}, \text{impeller} \right) \tag{1}$$

where Ne is the Newton number (alternativaly called power number) and the first and second numbers on the right-hand-side are the Reynolds number and the square of the Froude number, respectively. In Eq. (1) P is the power, N is the rotational speed in [rps] and the other quantities are in SI units. The geometrical parameters D, H, C and T are explained in Figure 1-a)

Froude number effects are not important because the baffles, and the low flow velocities near the fluid surface, help keep a flat free-surface.

The viscosity of non-Newtonian fluids is usually variable, therefore the issue of a characteristic viscosity η_c for the calculation of the Reynolds number in Eq. (1) arises. For stirred vessel flows this issue has been addressed long time ago by Metzner and Otto (1957) and Calderbank and Moo-Young (1959) who devised a strategy aimed at comparing *Ne- Re* data obtained under different geometrical conditions and with different impellers. The adopted strategy was inspired by that used to define an apparent viscosity in laminar pipe flow.

The characteristic viscosity η_c, which they also called apparent viscosity, is defined in such way that the *Ne-Re* relationship for non-Newtonian fluids coincides with the *Ne-Re* relationship for Newtonian fluids in the laminar flow regime, at identical rotational speeds and other flow conditions being equal. Metzner and Otto (1957) proceeded to relate the apparent viscosity with a characteristic shear rate and for that purpose assumed that the flow in the impeller region was characterised by an average shear rate which is linearly related to the rotational speed by

$$\dot{\gamma}_{AV} = kN \tag{2}$$

This is arguably correct but it is a convenient and simple assumption for engineering purposes and has since been adopted in the specialised literature. Cavadas and Pinho (2001) have recently measured the power consumption with very viscous solutions of CMC and xanthan gum to determine the coefficient k for the hyperboloid and arrived at $k = 48$ which is adopted in this paper.

The mean flow pattern in this stirred vessel is complex and three-dimensional but can be typified in the following sum of basic flow patterns: superimposed on a general rotating flow in the centre of the vessel, created by the impeller rotation, there is a vertical ascending movement of fluid along the vessel walls and a downwards motion at

the centre, in the vicinity of the impeller axis (Pinho et al, 1997). Between these two regions the flow is fairly weak as the fluid is entrained into one of them. This general pattern is characteristic of flows generated by axial impellers in combination with baffles, as discussed by Oldshue (1983).

One measure of this overall vertical motion is called the circulation flow rate $\dot{Q}_c$, which is the maximum flow rate obtained from integration of the measured axial velocities according to

$$\dot{Q}_c = \max \dot{Q}^+ \text{ or } \max \dot{Q}^- \quad \text{with } \dot{Q}^- = 2\pi \int_{r_{shaft}}^{r_{(u=0)}} r u_z(r) dr \quad \text{and} \quad \dot{Q}^+ = 2\pi \int_{r_{(u=0)}}^{r_{wall}} r u_z(r) dr \tag{3}$$

Obviously, conservation of mass ensures that both quantities are identical. $\dot{Q}_c$ is normalised into the circulating flow number Fl_c defined in Eq. (4) which can be combined with the power number of Eq. (1) to define efficiency numbers that allow comparison of different types of impeller. Here, two such ratios (E_2 and E_c) will be determined which are given by the expressions (5) and (6).

$$Fl_c = \frac{\dot{Q}_c}{ND^3} \tag{4}$$

$$E_2 = \frac{Fl_c^3}{Ne} \tag{5}$$

$$E_c = \frac{Fl_c^3}{Ne}\left(\frac{D}{T}\right)^4 \tag{6}$$

3. EXPERIMENTAL FACILITY AND INSTRUMENTATION

The stirred vessel is schematically represented in Fig. 1. The vessel consisted of a 292 mm diameter T stirred vessel in acrylic, which was mounted on a support standing directly on a 3-D milling table. The vessel allowed a maximum height H of liquid of 600 mm, but the present measurements refer to $H/T = 1$. The vessel was mounted inside a square trough filled with water that played a double role: it reduced the amount of refraction in the laser beams of the lasser-Doppler anemometer and it was also part of a heating and cooling circuit necessary to maintain a constant temperature in the bath. Within the tank, four 25 mm wide and 4 mm thick baffles were mounted at 90° intervals to avoid solid-body rotation of the fluid. The baffles were attached to small triangular connectors which separated them by 6 mm from the vessel wall, to eliminate the dead zones normally found behind the baffles. The bottom of the tank was flat and had a bearing embedded in it to support the drive shaft, thus minimizing shaft wobbling. Geometric details of the vessel and the coordinate system used are shown in Fig. 1-a).

The profile of the 100 mm diameter (D) hyperboloid impeller is plotted in detail in Fig. 1-b). The coordinates of the profile shown are listed in Table I. The impeller had transport ribs on the upper surface (rectangles of 7 x 3.6 mm^2) and the shear ribs at the bottom (rectangles of 5 by 3.6 mm^2). More details can be found in Höfken and Bischof (1993). The hyperboloid was mounted on a 12 mm shaft, which had a small 8 mm diameter recess where the hyperboloid was fixed. The impeller was positioned with an off-bottom clearance to vessel diameter ratio (C/T) of 1.3/30.

3.1 Power measuring system

A 600 W DC servomotor powered the impeller and was controlled by a variable power supply unit. A tachogenerator gave an electrical impulse proportional to the speed and controlled it together with an amplifier. The analog output, from 0 to 10 V, corresponded to a speed in the range 0 to 3,000 rpm. The speed could be kept constant with an uncertainty of around ±1 rpm and it never exceeded 600 rpm, except for very short periods of time, to avoid damage to the baffles.

The torquemeter, model T34FN/1 from HBM, had a full range torque of 1Nm and was free from friction losses because it consisted of two distinct components: a rotor (T34r40/1), where the strain gauge bridge was attached, was fixed to the shaft, and a stator (T34ST) which comunicated in frequency with the rotor. The output from the torquemeter fed an MGC amplifier from HBM, and its output, as well as that from the tachogenerator, was fed to a computer via an A/D converter. Purpose-built software gave all the results, namely, the rotational speed, the torque and the power.

Table 1- Coordinates of the impeller surface of the 100 mm diameter hyperboloid impeller.

x [mm]	6	6	7	8	10	12	14	16	18
y [mm]	38.4	32.4	27	24.2	21	18.5	16.5	14.5	12.7
x [mm]	20	22	26	30	34	38	42	46	50
y [mm]	11.1	9.6	7.2	5.3	3.6	2.2	1.4	1.0	0.6

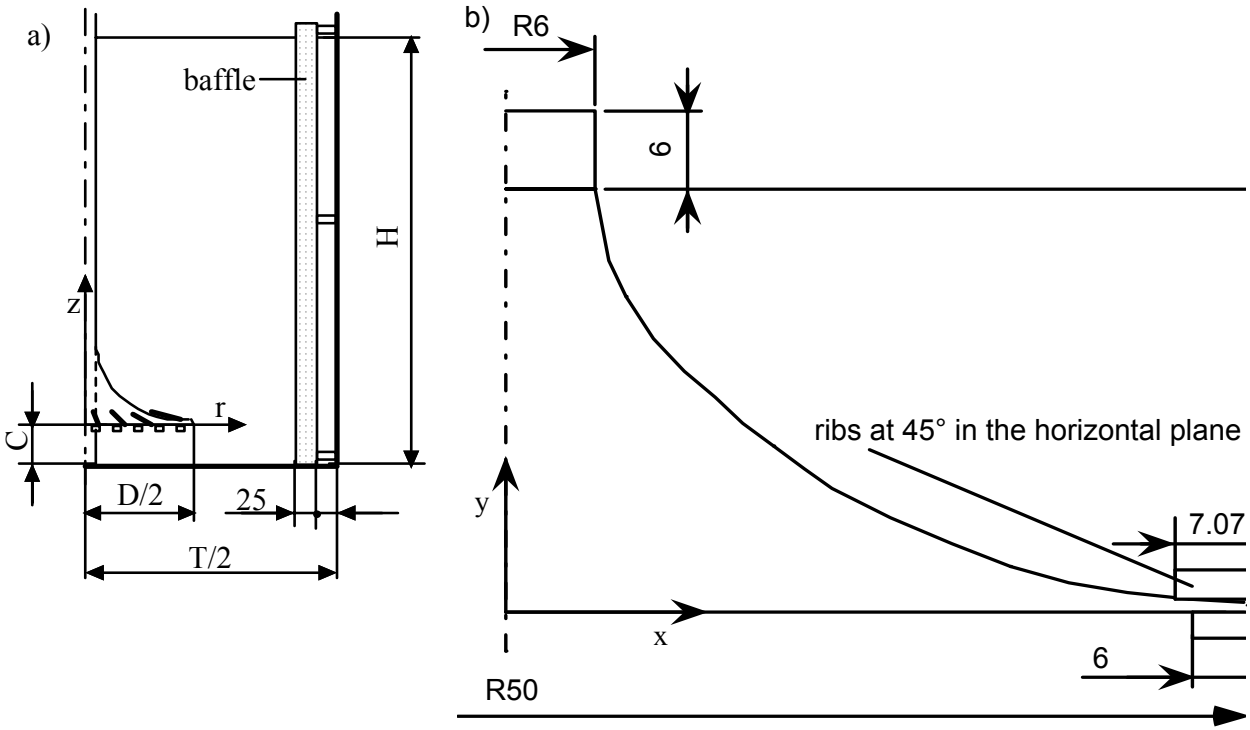

Fig. 1. Geometric representation of the stirred vessel and agitators:
a) the stirred vessel;
b) the hyperboloid impeller (see Table 1 for coordinates). $D/T = 1/3$; $H/T = 1$; $C/T = 1.3/30$.

The measured torque included the torque transmitted to the fluid and the torque loss absorved in the bearings. The torque loss was subtracted from the total torque to yield the net torque, after measurements were carried out with the water level just above the bottom bearing, but without touching the impeller. The uncertainty of the torque measurements is not constant and typically varied from about 7.5% to 0.3% when the impeller rotated from 100 rpm to 550 rpm, which corresponded to the minimum and maximum rotational speeds used for each fluid.

3.2 Laser-Doppler system

A 1-D Laser-Doppler anemometer was used to measure radial profiles of the axial velocity of the flows of some of the polymer solutions. The LDA system from Dantec was used in the forward scatter mode and the light source was an air-cooled, multimode 100 mW Ar-ion laser. The beam passed through a series of optical elements before the Bragg cell, where a frequency shift of 0.6 MHz was imposed. To improve the alignment of the optics and reduce the size of the control volume a pinhole section and beam expander, with an expansion factor of 1.95, were put before the 600 mm front lens.

The scattered light from titanium dioxide 3 μm mean diameter seeding particles, supplied by TSI Inc, was collected by the photo-multiplier before which stood an interference filter of 514.5 nm. For the non-Newtonian solutions it was not necessary to seed the flow with the TiO_2 particles. After being band-pass filtered the signal from the photo-multiplier was processed by a TSI 1990C counter operating in the single measurement per burst mode with a frequency validation setting of 1% in the 10/16 cycle comparison. A 1400 Dostek card interfaced the counter with a 80486 based computer which provided all the statistical quantities via a purpose-built software. The refraction of the laser beams in the plane walls of the trough and in the curved walls of the vessel was taken into account to correct the positioning of the control volume. Table 2 provides the main characteristics of the Laser- Doppler anemometer.

The measurements required for the circulating flow rate determination were carried out at locations far from the impeller where, for Newtonian fluids, the flow was found to be angle-independent by Pinho et al (2000). For the present more viscous fluids the measurements of the mean and rms values of the instantaneous velocity were obtained with 360° ensemble-averaged measurements from a sample size of 28,000 valid readings. This large sample was necessary for accurate results because of the low velocities and high levels of local turbulence encountered in the region.

Table 2- Main Characteristics of the Laser- Doppler anemometer in air at e^{-2} intensity.

Laser wavelength	514.5 nm
Measured half angle of beams in air	3.65°
Dimensions of measuring volume in air	
major axis	2.53 mm
minor axis	162 μm
Fringe spacing	4.041 μm
Frequency shift	0.6 MHz

4. FLUIDS

4.1 Fluid preparation

Measurements of the power consumption were carried out with nine aqueous polymer solutions based on three different polymers, but only with two of them (0.2% CMC and 0.2% XG) the pumping capacity was investigated. To all fluids, 0.02% by weight of the biocide Kathon LXE from Rohm and Haas was added to prevent bacteriological degradation. The fluids were the following where the concentrations are by mass:

- 0.2%, 0.4% and 0.6% solutions of the low molecular weight (6,000 g/mole) methyl hydroxyl cellulose, brand name tylose, grade MH10000K, from Hoechst. Tylose is a small molecule with a glucose based backbone, and more details can be found in Pereira and Pinho (1994);
- 0.2%, 0.3% and 0.4% solutions of moderate molecular weight (300,000 g/mole) carboxymethyl cellulose sodium salt, brand name CMC, grade 7H4C, from Hercules. CMC is a branched semi-rigid molecule, but is longer than the molecule of tylose. More details can be found in Escudier et al (2001) and Tam and Tiu (1989);
- 0.1%, 0.2% and 0.25% of the high molecular weight ($2x10^6$ g/mole) xanthan gum (XG), brand name Keltrol, grade TF from Kelco. Xanthan gum is a polysaccharide produced by the action of a bacteria and is also a semi-rigid, but long molecule. More details on this polymer can be found in Escudier and Smith (1999) and Lapasin and Pricl (1995).

All solutions were prepared with Porto tap water following the same procedure. The additives were added slowly to the water while being stirred, after which the mixture was agitated for a further 90 minutes. Then, the solutions rested for 24 hours to ensure complete hidration of the molecules, and prior to any rheological or hydrodynamic measurement the solutions were agitated again for 30 minutes to fully homogenise them.

4.2 Fluid rheology

Figures 2 to 4 plot the viscometric viscosity of the dilute solutions of tylose, CMC and xanthan gum as a function of shear rate, respectively. The least shear-thinning fluids are those made from tylose, as expected due to the low molecular weight. The xanthan gum solutions exhibit very strong shear-thinning (note the different scaling of Fig. 4) with the first Newtonian plateau not yet observed at the lowest measured shear rates in contrast to what is seen for all CMC and tylose solutions. At high shear rates, these same xanthan gum solutions become the less viscous, or as viscous as the thin 0.2% tylose solution.

Viscosity models were fitted to the measured data by a least-squares method. For the tylose and CMC solutions the simplified Carreau model (Eq. 7) was adopted since the data shows the low shear rate plateau followed by the power law region. For the xanthan gum solutions the Sisko model of Eq. (8) provided a better fitting. The parameters of the adjusted viscosity models are tabulated in Tables 3 and 4, respectively.

$$\eta = \mu_0 \left[1 + (\lambda_C \dot{\gamma})^2 \right]^{(n_C - 1)/2} \tag{7}$$

$$\eta = \mu_r \left(\lambda_s \dot{\gamma}\right)^{n_s - 1} + \mu_\infty \tag{8}$$

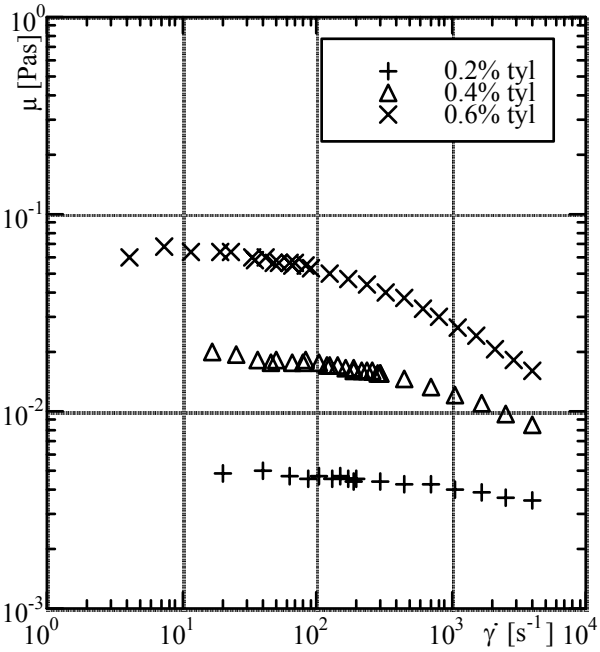

Fig. 2. Viscometric viscosity of the tylose solutions at 25°C.

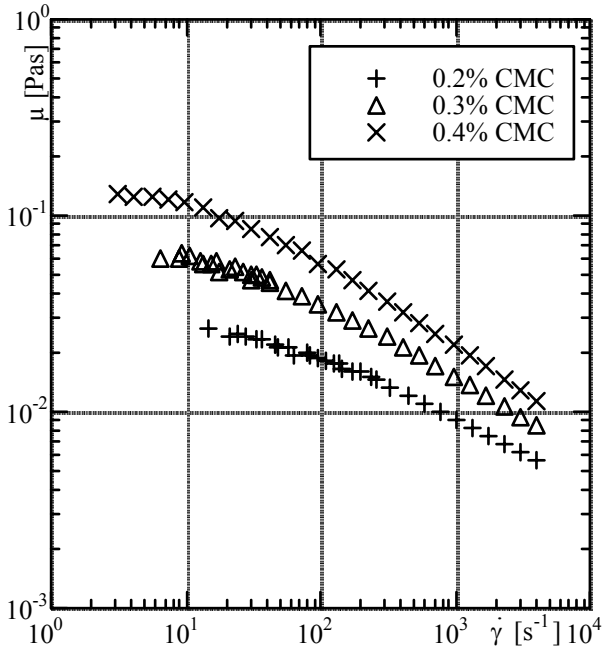

Fig. 3. Viscometric viscosity of the CMC solutions at 25°C.

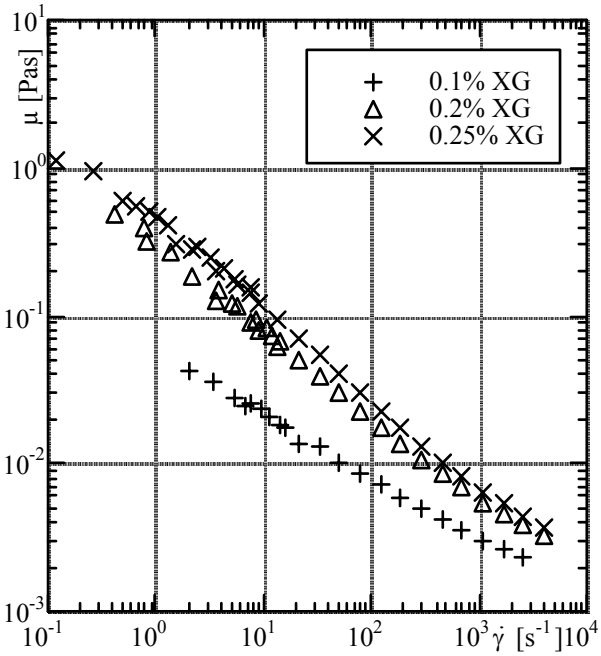

Fig. 4. Viscometric viscosity of the XG solutions at 25°C.

Table 3- Parameters of the adjusted simplified Carreau model.

Fluid	μ_0 [Pas]	λ_c [s]	n_c	$\dot{\gamma}$ [s^{-1}]
0.2% CMC	0.02652	0.03053	0.697	7-4031
0.3% CMC	0.08533	0.23517	0.717	3-4031
0.4% CMC	0.14097	0.11376	0.618	100-4031
0.2% tyl	0.00463	0.00377	0.900	40-4031
0.4% tyl	0.01865	0.00713	0.783	10-4031
0.6% tyl	0.06268	0.01468	0.697	8-4031

Regarding fluid elasticity, measurements in oscillatory shear flow for the more concentrated solutions are reported elsewhere. For the 0.6% tylose Coelho and Pinho (1998) found a basically viscous fluid with the ratio of loss over the elastic moduli $G''/G' \sim 3$ to 5 and a value of G' of 0.12 Pa at 10 Hz but the accuracy of the used rheometer was rather poor and the measurements were limited to the range of 5 to 20 Hz. Benefiting from more recent instruments Escudier et al (2001) confirmed and extended the results obtained by Coelho and Pinho (1998). The 0.4% CMC solution was more elastic than the 0.6% tylose and, in the range 0.01 to 50 Hz G''/G' decreased from 11 to 1.25 on increasing the frequency: $G' \approx 0.0024$ Pa and $G'' \approx 0.027$ Pa at 0.1 Hz, and $G' \approx 3.2$ Pa and $G'' \approx 4.0$ Pa at 50 Hz, respectively.

The larger and more branched xanthan gum molecules naturally yielded more elasticity and viscosity in this near-rest rheological flow. At 0.01 Hz, $G' \approx 0.02$ Pa and $G'' \approx 0.048$ Pa, but at a frequency of 50 Hz the elastic stress was higher than the viscous stress since $G' \approx 3.2$ Pa and $G'' \approx 1.8$ Pa.

Table 4- Parameters of the adjusted Sisko model.

Fluid	μ_r [Pas]	λ_s [s]	μ_∞ [Pas]	n_s	$\dot{\gamma}$ [s^{-1}]
0.1% XG	1.86	1970	0.001	0.543	3-2700
0.2% XG	31.47	2909	0.001	0.417	0.5-4031
0.25% XG	98.54	1700	0.001	0.326	0.1-4031

5. RESULTS AND DISCUSSION

5.1 Power consumption

Figures 5 a) to c) plot the power number as a function of the generalised Reynolds number of Otto and Metzner (1957) for the tylose, CMC and xanthan gum solutions, respectively. In each graph the solid line represents the best fit to the experimental measurements of Cavadas and Pinho (2001) obtained with four Newtonian mixtures of glycerin and water. The plots show a decrease in the Newton number of about 13%, especially for the CMC solutions, but the decrease is absent from the less elastic 0.2% tylose.

In general, at Reynolds numbers in the range 10^3 to 10^4 the power number for the polymer solutions attain values of the order of 0.7 and less, whereas for Newtonian fluids it is higher than the asymptotic high Reynolds number value of 0.81. For the tylose solutions (Fig. 5-a) the power number increases with Reynolds number at the upper limit of this range and seems to approach the Newtonian curve. Note that the tylose solutions are those having a rheology closest to the Newtonian, both in terms of viscosity and elasticity. For the CMC, however, although there is a slight tendency for *Ne* to increase with *Re*, the variation does not seem sufficient for the power number to attain the Newtonian curve.

Finally, for the xantham gum the power number starts with values lower than those of the Newtonian fluids at Reynolds numbers around 3,000, then it increases and at Reynolds numbers in excess of 20,000 the power number of the 0.1% XG is close to the Newtonian value but still lower. A feature common to all plots is that the less concentrated solution have a tendency to higher power numbers at the low end of the Reynolds number range.

The lower power numbers of the polymer solutions were not unexpected. These same solutions are known to exhibit drag reductions in excess of 40% in fully-developed turbulent pipe flow, Escudier et al (1999). Whereas the flow in the pipe is dominated by wall-effects, here the wall that has an impact on power consumption is the impeller, but the molecules only stay in its boundary-layer for a very short period of time. Nevertheless, it is still remarkable that about 10% of power reduction is observed with these solutions.

5.2 Flow circulation

Since the hyperboloid impeller is close to the bottom of the vessel (*C/T*= 1.3/30, see Fig. 1-a), the measurements of the axial velocity component were carried out at various horizontal planes above its base plane, in the range *z/R*= 0.6 to 2.0. It was in this region that Pinho et al (1997) found the highest axial flow rates, in particular near *z/R*=1. The present axial velocity measurements were carried out with water, to compare with Pinho et al (1997), and more extensively with the solution of 0.2%XG to analyse the polymer effect and less so for a solution of 0.2% CMC. No velocity measurements were carried out with other solutions and all velocities are normalised by the impeller tip speed U_{tip}.

A first impression of the differences between the Newtonian and non-Newtonian flow fields can be grasped from inspection of Figure 6 measured at *z/R*= 1.4. In the center of the vessel the negative velocity values of the

descending flow are similar but the flow is slightly slower for the xanthan gum solution. In the wall jet the peak velocity of the ascending flow is again higher (faster) for the water and occurs closer to the wall than for the polymer solution. However, the main difference is in the turbulent flow field: across the whole vessel radius the normalised axial turbulence for the xanthan gum solution is less than half that of the water flow. The turbulence of the xanthan gum is so low that its rms profile becomes very sensitive to mean gradient broadening effects near the vessel wall. The Newtonian profiles were compared with the data from Pinho et al (1997) and the differences were negligible and within the experimental uncertainty.

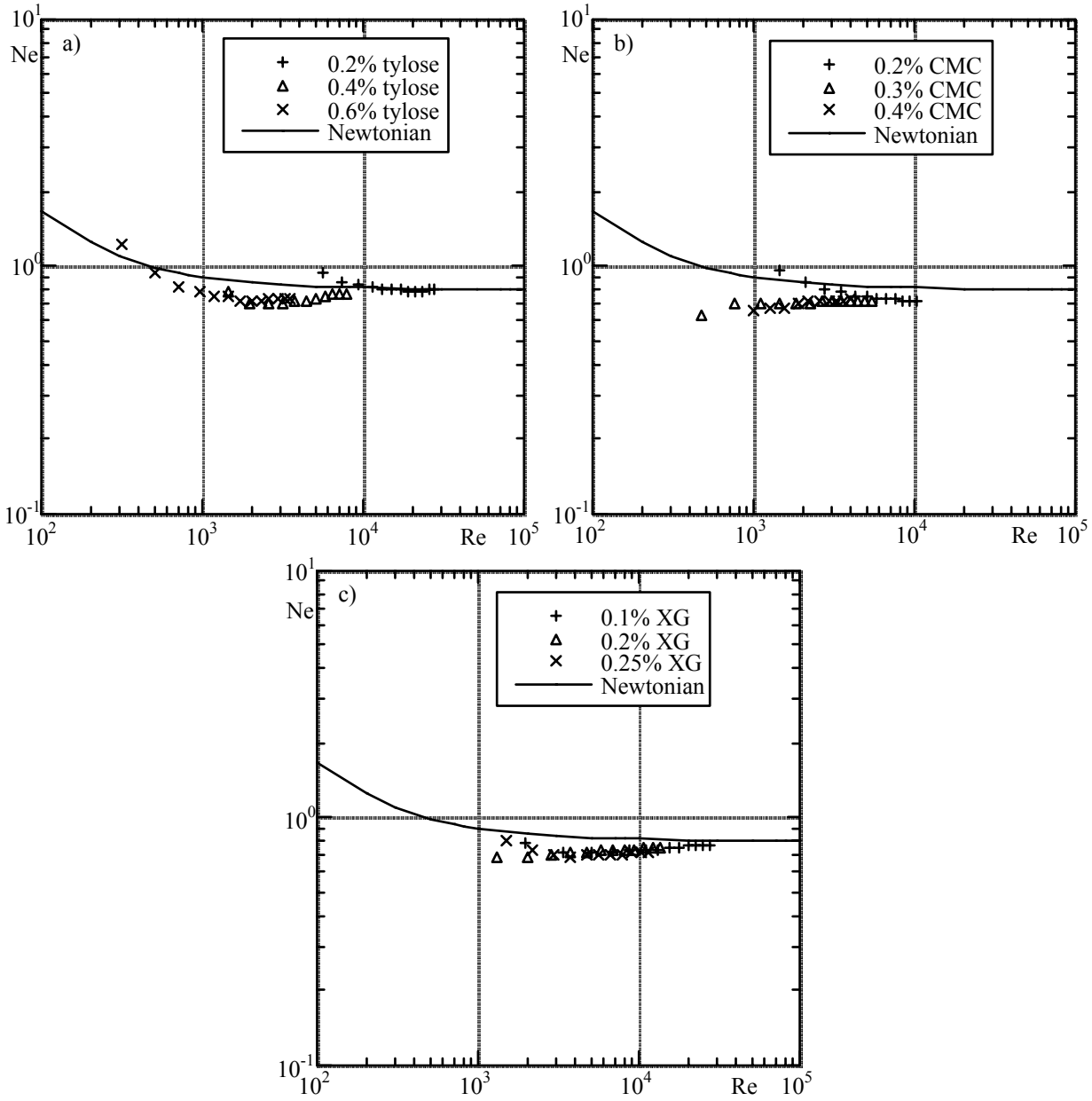

Fig. 5. Variation of the Newton number with the Reynolds number in stirred vessels agitated by one hyperboloid impeller in the standard configuration ($H/T = 1$, $D/T = 1/3$):
a) Tylose;
b) CMC;
c) xanthan gum. Line represents equation fitted to Newtonian data by Cavadas and Pinho (2001).

From these profiles the axial flow rate was calculated in both the ascending (wall jet) and descending flow regions (centre of the vessel) and the differences were found to be less than 10%. Since it was not possible to measure very close to the impeller with forward scatter, and because it was not possible to obtain valid LDA signals in backscatter for the less clear xanthan gum and CMC polymer solutions, it was decided to perform the remaining measurements of axial velocity, aimed at determining the circulating flow rate, only in the wall jet region. This required careful measurements in the wall region because of its large contribution to the flow rate.

The Newtonian flow at the wall jet is compared at two diferent Reynolds numbers in Figure 7. Both cases pertain to high Reynolds numbers where the turbulent flow is well developed and, consequently, the dependence of the normalised mean and rms velocities is very weak and only detected in the slightly higher peak values at the highest Reynolds number. In this and in subsequent Figures, the velocity data is plotted only in this wall jet region.

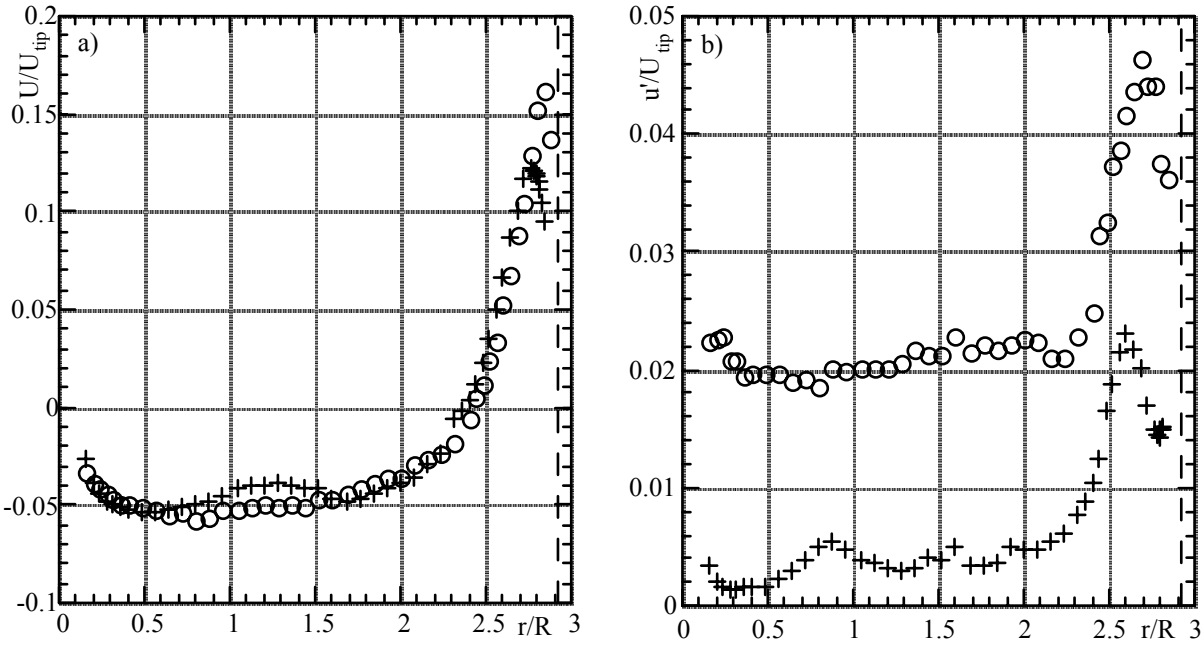

Fig. 6. Radial profiles of the mean (a) and rms (b) axial velocity component at z/R= + 1.4 for: water, Re= 52,400 (O); 0.2% XG, Re= 8,210 (+). Vertical dashed line marks vessel wall location.

Next, Figure 8 compares the wall jet at *z/R*=1 for a Newtonian flow at 300 rpm and the 0.2% xanthan gum flow at 500 rpm, but the corresponding Reynolds numbers differ by a factor of 6. At speeds in excess of 650 rpm unnecessary strain was put into the perspex baffles and, for protection, these high speeds were only used during the short periods required for the power measurements, but not for velocity measurements. The picture described in Figure 6 emerges again: the mean flows are not very different but the turbulence is basically half of that found with water and the above-mentioned mean gradient effect is now more clear which indicates that the true turbulence is smaller than shown.

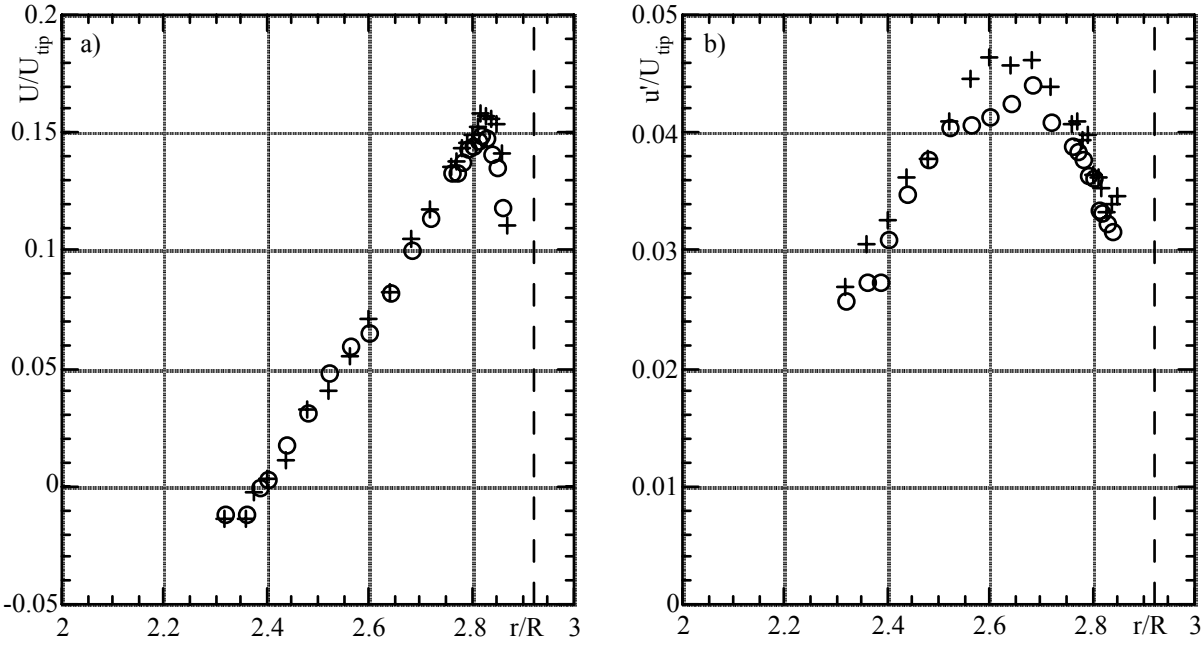

Fig. 7. Radial profiles of the mean (a) and rms (b) axial velocity component at the wall jet for water flow at z/R= + 1: Re= 56,200 (O); Re= 93,600 (+). Dashed line marks vessel wall location

The development of the wall jet with height is represented in Figure 9-a) which plots the radial variation of the normalised axial mean velocity for increasing values of *z/R*. As *z/R* progresses from 0.6 to 1.8 the peak velocity near the wall decreases by a factor of a third, from 0.16 to 0.11, and the normalised width δ / R of the jet increases from 0.44 to 0.65. The corresponding rms profiles show a decreasing turbulence with *z/R* which can be attributed to a combination of two effects: on one side the turbulence in the flow, which is mostly generated in the impeller region, is probably decreasing as the fluid moves away from the bottom of the vessel and, secondly, the steeper mean velocity profiles found at lower *z/R* generate higher values of gradient broadening which decreases on moving upwards. Since the wall jet is a region of turbulence production, and the different curves pertain to locations not far from each other, we believe that the differences seen here are basically related to the gradient broadening effect rather than caused by a local decay in turbulence. Nevertheless, these differences occur because of the low turbulence intensity of the polymer solution flow as it reaches the wall jet. Whether this low turbulence is due to a lower turbulence production in the impeller region or a faster dissipation subsequently, or both, requires a more extensive investigation.

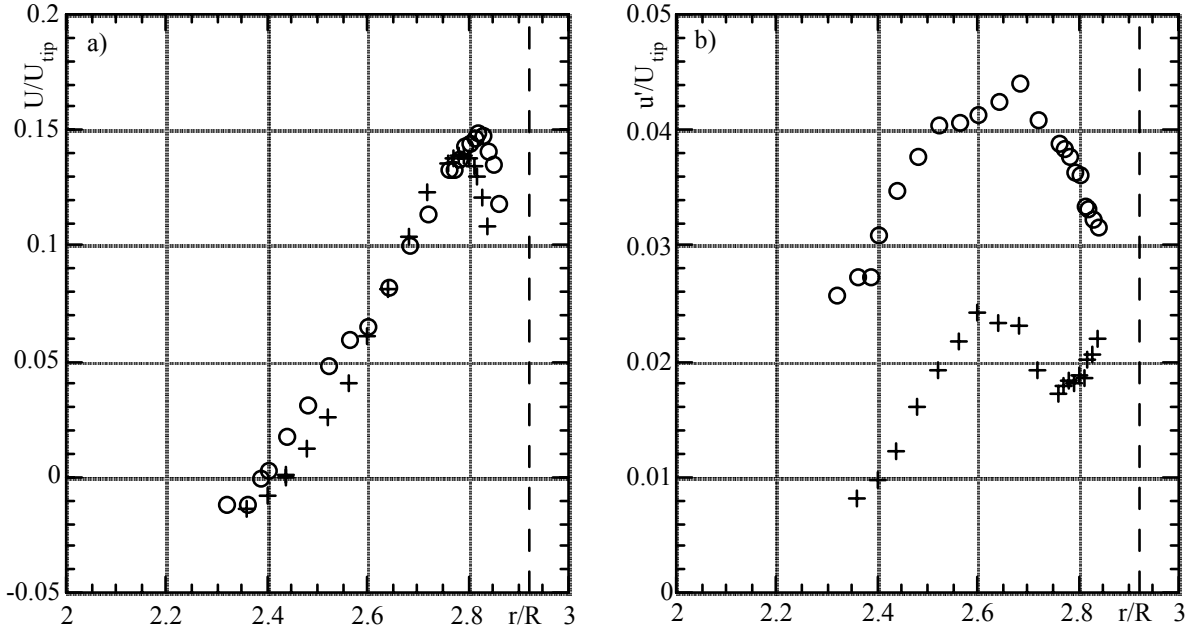

Fig. 8. Radial profiles of the mean (a) and rms (b) axial velocity component at the wall jet and z/R= + 1.0 for: water, Re= 52,400 (O); 0.2% XG, Re= 8,210 (+). Vertical dashed line marks vessel wall location.

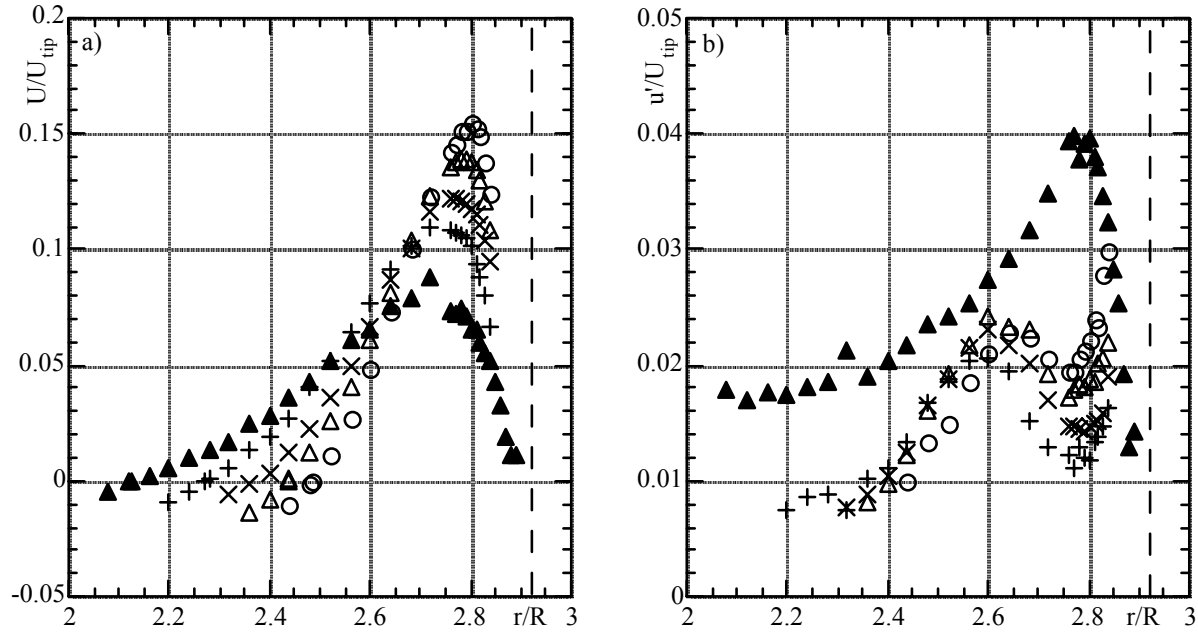

Fig. 9. Effect of height and polymer additive on the radial profiles of the mean (a) and rms (b) axial velocity component at the wall jet for 0.2% XG at Re= 8,210: z/R=0.6 (O); z/R=1 (Δ); z/R=1.4 (X); z/R=1.8 (+); 0.2%CMC and Re= 5,430 at z/R=1 (solid Δ). Vertical dashed line marks vessel wall location.

Figure 9 includes one profile at z/R=1 for a 0.2% CMC solution, but at a lower Reynolds number of 5430 and it should be compared with the corresponding profile for the xanthan gum at z/R=1. In spite of its lower Reynolds number the CMC profiles are typical of a more turbulent flow, ie, the jet is wider and less peaky and the normalised rms profile is well above all the profiles for the xanthan gum solution. The peak normalised rms for the CMC is 0.04 which is only 10% less than that seen in Figure 8 for the water flow. Since the mean velocity profile is less steep than for the xanthan gum the gradient broadening effect is less severe and this shows well particularly near the wall where the tendency for a rise in rms only appears very close to the wall.

The obvious question is why the behaviour of the CMC and xanthan gum solutions are so different? At this stage one can only speculate but to this difference certainly one must take into account the viscosity variation of both fluids at low shear rates (cf Figs 3 and 4). Whereas the 0.2% CMC tends to a Newtonian plateau of about 0.03 Pas (0.0265 Pas according to the data fitting), the low shear rate viscosity of the 0.2% xanthan gum solution is, by contrast, very high, with a value of 0.3 Pas at $\dot{\gamma}$ =1 s^{-1}. It is known, from the Newtonian results of Pinho et al (1997, 2000), that at the inner edges of the bottom and wall jets the flow is rather weak. By their nature, shear-thinning fluids will accentuate this pattern and especially so the xanthan gum solutions which have a very intense shear-thinning. Besides, in these low velocity regions the turbulence dissipation is bound to be very intense and again the turbulence must decay faster for the xanthan gum solution than with the CMC solution on account of the viscosity at low shear rates.

5.3 Efficiency

The data presented in Figures 7 to 9 allowed the calculation of the axial flow rate $\dot{Q}^{+}$ in the ascending flow region (positive velocities), the maximum of which is $\dot{Q}_c$ and is used to define the circulating flow number according to the formulae in Section 2. Whereas for the water flow Fl_c = 0.51 to 0.54 for Re= 50,000 to 90,000, in agreement with the value of 0.57 obtained by Pinho et al (1997) within the experimental uncertainty, there was a decrease of about 20% for both the 0.2% CMC and 0.2% XG polymer solutions which showed values of Fl_c = 0.42 and 0.45, respectively.

Since the decrease in Fl_c due to the addition of polymer was higher than the corresponding decrease in Ne, the two efficiency ratios were reduced in relation to that for Newtonian fluids. For the water flows $E_2 = 0.2$ and $E_c = 0.0025$ matching the values of Pinho et al (1997), whereas for the CMC and xanthan gum flows E_2 varied from 0.1 to 0.12 and E_c from 0.0013 to 0.0014. This important reduction in efficiency, of the order of 50%, together with the reduced turbulence in the wall jet for the xanthan gum solution and its implications regarding mixing quality, raises questions to the usefulness of the hyperboloid as a mixer in waste water treatment plants. As has been demonstrated by Monteiro and Valente (1996), sludges found in waste water treatment plants usually have a yield stress. Although yield stress fluids were not used in the present investigation, the xanthan gum solution has a very wide range of shear rates where the fluid is strongly shear-thinning and so it approaches well in this flow, from an engineering point of view, the expected behaviour for yield stress fluids.

6- CONCLUSIONS

Measurements of the power consumption were carried out with aqueous solutions of tylose, CMC and xanthan gum in concentrations ranging from 0.1% to 0.6% by weight. The tylose solutions were the less shear-thinning with a wide first Newtonian plateau whereas the xanthan gum solutions were so strongly shear-thinning that at shear rates lower than $1s^{-1}$ the viscosity was still varying significantly. For all solutions the power measurements showed a reduction relative to the Newtonian values, at identical Reynolds numbers in the range 10^3 to $3x10^4$. This power reduction was stronger with the more concentrated solutions, for each polymer, but never exceed 13%.

For the measurements of the mean and rms axial velocity along the radius of the vessel only the solutions of 0.2% xanthan gum and 0.2% CMC were investigated, together with water for comparison purposes. The measurements were carried out in planes above the impeller, at z/R between 0.6 and 1.8, and showed that the mean flow of the non-Newtonian solutions did not change significantly and resulted in circulating flow rates that were 25% lower than the corresponding quantity for Newtonian fluids, with the xanthan gum was more affected. However, the rms profiles showed a dramatic difference of behaviours: whereas the turbulence of the xanthan gum solution was less than half of the turbulence of the water flow both in the wall jet and in the center of the vessel, for the CMC the difference was merely 10% in the wall jet. It was speculated that this dramatic difference between the behaviours of the two polymer solutions was attributed to their different low shear rate viscosity. In fact, although at high shear rates the 0.2% xanthan gum solution is less viscous than the 0.2% CMC solution, at the low shear rates that prevail in the slow flow regions of the vessel the viscosity of the XG solution is ten times larger than that of the CMC solution.

REFERENCES

Calderbank, P.H. and Moo-Young, M.B. (1959) The prediction of power consumption in the agitation of non-Newtonian fluids. *Trans. Inst. Chem. Engr.*, 37, pp 26-33.

Cavadas, A.S. and Pinho, F.T. (2001) Power consumption of polymer solutions in a stirred vessel powered by an hyperboloid impeller. Paper 24905.pdf in *CD-ROM Proceedings 3, Fluid Mechanics, Rheology and Fluid Mechanics of Non-Linear Materials Symposium, ASME International Mechanical Engineering Congress & Exposition*, 11th-16th November, New York, NY, USA.

Coelho, P.M. and Pinho, F.T. (1998) Rheological behaviour of some dilute aqueous polymer solutions (in portuguese). *Mecânica Experimental* , 3, pp 51-60.

Escudier, M.P., Gouldson, I.W., Pereira, A.S., Pinho, F.T. and Poole, R.J. (2001) On the reproducibility of the rheology of shear-thinning liquids. *J. Non-Newt. Fluid Mech.*, 97, pp 99-124.

Escudier, M.P., Presti, F. and Smith, S. (1999) Drag reduction in the turbulent pipe flow of polymers. *J. Non-Newt. Fluid Mech.*, 81, pp 197-213.

Escudier, M.P. and Smith, S. (1999) Turbulent flow of Newtonian and shear-thinning liquids through a sudden axisymmetric expansion. *Exp. in Fluids*, 27, pp 427-434.

Höfken, M., Bischof, F. and Durst, F. (1991) Novel hyperboloid stirring and aeration system for biological and chemical reactors. *ASME -FED- Industrial Applications of Fluid Mechanics*, 132, pp 47-56.

Höfken, M., Zähringer, K. and Bischof, F. (1994) Stirring and aeration system for the upgrading of small waste water treatment plants. *Water Science and Technology*, 29, pp 149-156.

Ismailov, M., Schäfer, M., Durst, F. and Kuroda, M. (1997) Turbulent flow pattern of hyperboloid stirring reactors. *Journal Chem. Eng. Japan*, 30, pp 1090-1097.

Lapasin, R. and Pricl, S. (1995) *Rheology of Industrial Polysaccharides: Theory and Applications*. Blackie Academic and Professional, London.

Metzner, A.B. and Otto, R.E. (1957) Agitation of non-Newtonian fluids. *AIChEJ*, 3, pp 3-10.

Monteiro, P. and Valente, J.T. (1996) Flow characteristics of anaerobic digesting sludges. *Proceedings of the 18th International Conference on Slurry Handling and Pipeline Transport- Hydrotranssport 18-* edited by J F Richardson, South Africa, 3-5 September, BHR Group Conference Series, pp 3-20

Nouri, J.M. and Whitelaw, J.H. (1994) Flow characteristics of hyperboloid stirrers. *Can. J. Chem. Eng.*, 72, pp 782-791.

Oldshue, J.Y. (1983) *Fluid Mixing technology*. McGraw-Hill Book Company, New York.

Pereira, A.S. and Pinho, F.T. (1994) Turbulent pipe flow characteristics of low molecular weight polymer solutions. *J. Non-Newt. Fluid Mech.*, 55, pp 321-344.

Pinho, F.T., Piqueiro, F.M., Proença, M.F. and Santos, A.M. (1997) Power and mean flow characteristics in mixing vessels agitated by hyperboloid stirrers. *Can. J. Chem. Eng.*, 75, pp 832-842**.**

Pinho, F.T., Piqueiro, F.M., Proença, M.F. and Santos, A.M. (2000) Turbulent flow in stirred vessels agitated by a single, low-clearance hyperboloid impeller, *Chem. Eng. Sci.* 55 (16), pp 3287-3303.

Tam, K.C. and Tiu, C. 1989. Steady and dynamic shear properties of aqueous polymer solutions. *J. Rheology* 33 (2), pp 257-280.